Data-Enabled Research Training and Development Sprints (DARTS) 2025 Report

---

Multimodal Deep Learning of PV Module Images

David J. Tang[2], Sebastian J. Noel[1], Isaac H. LaRose[1], Dawn Balaschak[1], Ezzat Boukhary[1], Andres O. Sainz[1,4], Joseph M. Raby[1,4,6], Kristopher O. Davis[3,4,5,6]

1. Department of Computer Science and Engineering, University of Central Florida, Orlando, Florida, U.S.A.
2. Department of Mathematics, University of Central Florida, Orlando, Florida, U.S.A.
3. Department of Materials Science and Engineering, University of Central Florida, Orlando, Florida, U.S.A.
4. Resilient, Intelligent and Sustainable Energy Systems (RISES) Research Center, University of Central Florida, Orlando, Florida, U.S.A.
5. CREOL, the College of Optics and Photonics, University of Central Florida, Orlando, Florida, U.S.A.
6. Florida Solar Energy Center (FSEC), University of Central Florida, Cocoa, Florida, U.S.A.

Corresponding Author Email Address:
da274409@ucf.edu
se129568@ucf.edu
is992883@ucf.edu
br647907@ucf.edu
ez658256@ucf.edu
an660384@ucf.edu
jo638875@ucf.edu
kristopher.davis@ucf.edu

Keywords: photovoltaic modules, deep learning, multimodal, electroluminescence, ultraviolet fluorescence, current, voltage, wavelet transform, LSTM, MLP, defect detection, solar energy degradation, machine learning, k-means.

Abstract: Photovoltaic (PV) modules are prone to performance loss from microstructural defects that occur during manufacturing, transport, and long-term use. Accurate and scalable tools for assessing these defects are essential for improving module reliability, lowering maintenance costs, and enabling wider adoption of solar energy. This study investigates whether image-based features from electroluminescence (EL) and ultraviolet fluorescence (UVF) can be used to predict electrical performance metrics such as current, voltage, and power output. We constructed the M55 Universal Dataset by aligning EL, UVF, and IV measurements at the cell level, incorporating 2,075 image samples with matching defect and performance data. We applied unsupervised K-means clustering to explore data structure, followed by a Multilayer Perceptron (MLP) trained on 871 EL samples. Crack defects yielded the highest predictive value with an R^2 of 0.53 and MAE of 0.89. In contrast,

models trained on UVF classification data (78 samples) performed poorly due to limited coverage. For time-series prediction, we applied a Long Short-Term Memory (LSTM) model to IV signals. Wavelet preprocessing improved R^2 from 0.09 to 0.39 for current and from 0.51 to 0.77 for voltage. This work also introduces a reusable image processing and modeling pipeline packaged in a foundational codebase, supporting future PV degradation research using multimodal imaging.

1 Introduction

As the world continues to shift towards the use of renewable energy sources due to concerns about the environmental impact of nonrenewable energy, solar energy, an abundant and sustainable resource, has emerged as a leading alternative. Ensuring that solar energy production remains reliable over time is essential to supporting this transition.

Photovoltaic (PV) technology continues to expand as industries seek better ways to generate clean power. Performance measurements such as electroluminescence (EL), ultraviolet fluorescence (UVF), and current-voltage (IV) curves are commonly used to characterize PV cells and compare module performance. Although UVF was once a niche technique mainly used to evaluate polymer components, its popularity has grown significantly since 2017. Unlike EL, UVF does not require disconnecting modules from the circuit, making it more practical for field deployment [1, 2].

Earlier models helped shape the foundation of our research. In 2012, Tsai et al. introduced a Fourier image reconstruction method to detect line- and bar-shaped EL defects [3, 4]. After creating a model that can perform effectively (with small cracks, breaks, and finger interruptions) that only took 0.29 seconds to inspect a multicrystalline solar cell image (550x550 pixels), deep learning began to become popular [3, 4]. However, as Chen et al. found that deep learning takes a lot of training samples and labeled data, computation began to become more prevalent, as it favored speed [5]. Following suit, Tseng et al. used a spectral clustering model to identify and classify contact fingers as interrupted or not with a boastful 99% accuracy, but it was not a broad model. The model was limited to but one PV cell defect: finger interruption [6].

However, most of the data in the previous models used EL data. In 2025. Colvin et al. points out that there are several features that UVF can see that are otherwise invisible to other techniques, or would be destructive [1]. They also found that UVF can detect if cells operate at higher temperatures, or have at some point while running [1]. Sina et al. also focused on UVF, creating a pipeline to take a photo contained several modules and cropping them individually into cells (and correcting their orientation/perspective). The result would then be put through a network classifier and their leading model achieved an F1 score of 0.93 while processing 240 images per second [7]. The UVF would be an incredible advantage as it would be able to be combined with the EL data in order to have a more in depth record of every cell in

order to detect not just the defect, but the power and temperature the cell was producing throughout use.

In summary, many works have built off of one another, or diverged into separate ideas. Some built models to detect UVF data, while others focused on EL data. Some works even succeeded in having high accuracy in detecting a defect, but our goal was to combine it all into one; we wanted to build a model that could look at both EL and UVF data AND have high accuracy not only in classifying defects, but to figure out which was the most damaging. Our benefit is that we no longer lack the limited training data, as Fioresi et al. made the 17,064 EL images and Sina et al made the 1447 labeled and 53264 unlabled UVF images public, so we could create a deep learning model based on EL and UVF, allowing us to see both the EL data, and what would be otherwise invisible without the UVF [4, 7].

A few questions and goals we wanted to answer and accomplish with our research that would have a lasting impact on the future of photovoltaics are: Constructing a Universal M55 Data Set, including a 1-1-1 relationship, finding the best image method for predicting performance, and concluding which defect is the most valuable for predicting performance

In summary, our primary objective was to improve the energy conversion efficiency of photovoltaic (PV) modules by identifying and classifying the defect types that seemed to most greatly impair power output. To achieve this, we created a deep learning framework, looking into K-means clustering, a Multi-layer Perceptron (MLP), and a Long Short-term Memory learning models that leverage both electroluminescence (EL) and ultraviolet fluorescence (UVF) imaging modalities to detect, classify, and compare defects across the PV cells.

2 Dataset

The original M55 dataset consisted of separate data sources: IV measurements (561 rows), EL measurements (1,309 rows), and a larger EL defect dataset containing 34,633 cell-level entries. However, these resources were not consistently aligned in time or across module serial numbers. The merged IV-EL dataset contained only 561 matched rows. Meanwhile, the cell-level defect data included multiple time points for each module, grouped by serial number. In addition, there is an abundance of crack defects compared to the other defects (contact, interconnect, corrosion).

To address these inconsistencies, we constructed a unified dataset (M55 Universal Dataset) by integrating IV, EL, UVF classification, and defect percentage data. While some missing data remained (current and voltage has 50 rows missing EL defects and 114 rows missing for UVF defects), this version of the dataset provided a more structured and consistent foundation for multimodal modeling and time-series experimentation. The data was sorted by serial number and timestamp.

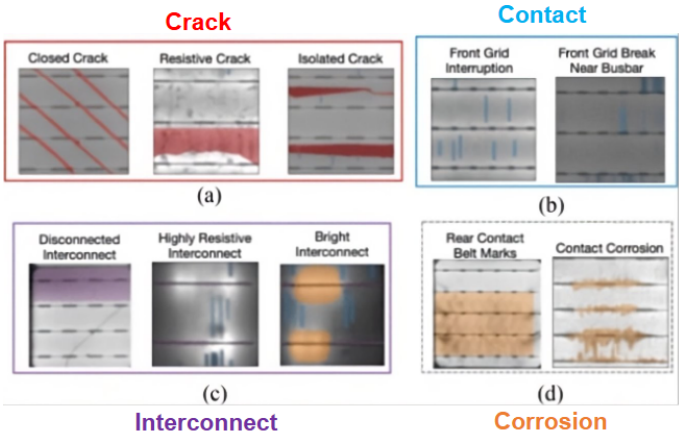

Fig. 1: EL defects

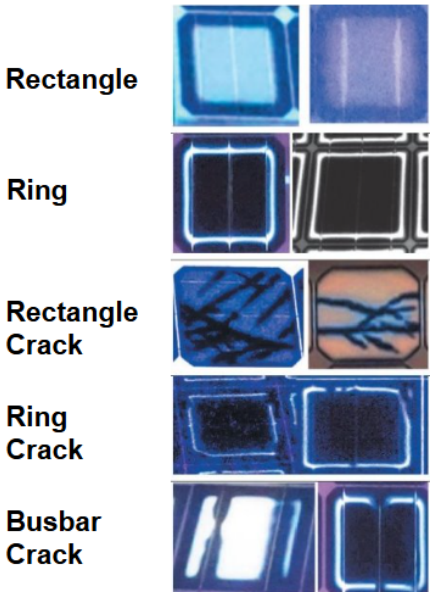

Fig. 2: UVF defects

3 Analysis Methods and Workflow

Image Processing and Defect Segmentation

Initial analysis required a multi-stage preprocessing pipeline for the preparation of the M55 PV image dataset. We employed a series of image processing scripts, like Sina et al., upon their supplied unabled UVF images into our workflow to accomplish this [7]. This began with background removal to isolate the module, gamma correction to increase the visibility of defects, and individual

cell cropping for detailed analysis. Following that, the cells were then stitched back together, and GIFs were generated to visualize the results.

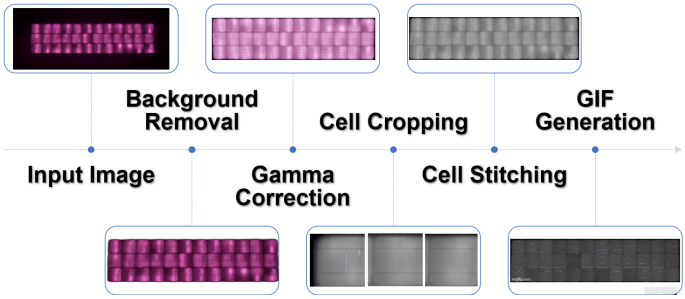

Fig. 3: The transformation from image to processed GIF

Subsequent to preprocessing, cells were then segmented for the quantification of their defect percentages. This also allowed for the creation of masks over defective areas, segmentation pixel counting for degradation metrics, and exportation of defect data into a CSV. To streamline the workflow and ensure reproducibility, a Marimo notebook was utilized for the processing these M55 modules. Providing the full image processing pipeline and several defect segmentation options for various analytical approaches. A Foundational Package that encompasses all the scripts we used and produced (including image processing, defect segmentation, and power loss correlation) was then established to enhance organization and promote future research.

Clustering for Structural Insights

We first applied K-means clustering as an unsupervised method to explore whether modules can be grouped based on their natural electrical characteristics and defect patterns. While not intended for prediction, this exploratory step provided insight into the underlying structure of the data and informed our feature selection strategy for supervised models. K-means works by partitioning the dataset into k clusters, where each data point belongs to the cluster with the nearest mean. The algorithm iteratively updates cluster centroids and assignments to minimize the variance within each cluster. This made it well-suited for revealing natural groupings in our unlabeled dataset.

Static Prediction using MLP

Next, we trained a Multilayer Perceptron (MLP) model to predict current and voltage based on defect features alone, such as EL defect percentages and UVF classifications. MLPs do not capture temporal dependencies, making them appropriate for the aggregated and static nature of available defect

data. This served as a baseline for understanding how informative individual defect modules were, independent of time. An MLP is a feedforward neural network composed of fully connected layers with nonlinear activation functions, typically used to approximate complex input-output relationships. Our model learned to map the defect characteristics of each module to corresponding electrical measurements, providing insight into the predictive power of defect patterns alone, without historical context.

Data Preprocessing and Temporal Challenges

To enable time-series modeling, we aggregated IV and EL data by unique combinations of date, time, and serial number, resulting in 921 rows. The UVF data were similarly grouped, yielding 201 rows. However, due to measurement inconsistencies and data gaps (such as missing time records or one sampling type, such as UVF, occurred more often, or poor environmental conditions), the resulting time series for each module remained irregular and sparse.

We experimented with several interpolation techniques to generate pseudo-regular time intervals, including linear interpolation, which fills missing values by drawing a straight line between known points, and forward fill, which carries the last known value forward until a new one is available. While simple to implement, linear interpolation often oversimplified the signal behavior, especially in regions with non-linear fluctuations in voltage and current. We also explored Fast Fourier Transform (FFT), a method that decomposes signals into their frequency components, aiming to reconstruct missing segments based on dominant periodic patterns. However, this approach proved effective in only a small subset of cases, primarily due to the non-periodic and unevenly sampled nature of the data. As a result, FFT was not used in the final modeling pipeline.

Wavelet Transform and LSTM Modeling

Given the presence of damped oscillations and transient behaviors in the current and voltage signals, we applied wavelet transforms, a time-frequency analysis method that decomposes signals into localized components at multiple scales. This allowed us to reduce noise while preserving critical signal features such as spikes or sudden changes. The resulting transformed signals retained localized temporal behavior and simplified patterns, making the data more suitable for sequential learning.

We initially trained a Long Short-Term Memory (LSTM) neural network, a type of recurrent neural network (RNN) designed to capture long-term dependencies in sequential data. Under the simplifying assumption of uniformly spaced time intervals, we used the LSTM to assess the baseline performance in predicting voltage and current. This approach allowed us to evaluate whether temporal trends in electrical behavior could be effectively modeled. As shown in the results section, wavelet preprocessing led to a significant improvement in predictive accuracy compared to using raw signals.

After establishing this baseline, we experimented with incorporating the actual irregular time intervals present in the data set. However, because of the sparsity and inconsistency of the measurements, this approach proved difficult to implement reliably. These findings suggest that while wavelet-enhanced LSTM architectures are promising, their full potential would be better realized in datasets with consistent, densely sampled time-series measurements.

4 Findings: Results and Discussion

4.1 K-means Clustering

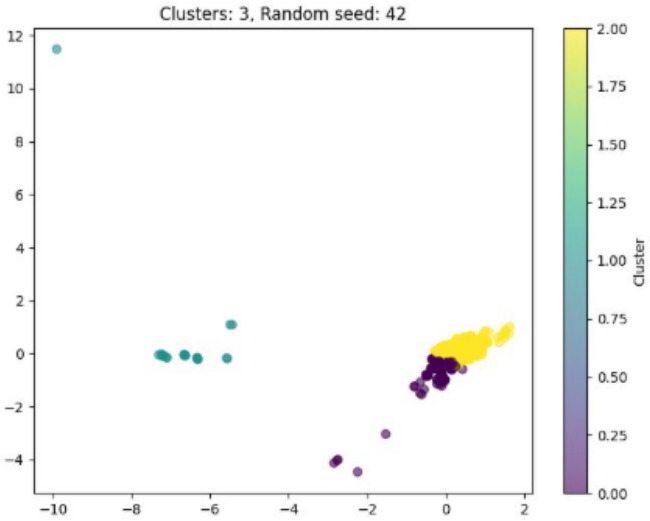

Fig. 4: Initial exploratory clustering based on current, voltage, and four EL defect types.

4.2 MLP (EL Defect Percentages Data)

Following interpolation and aggregation, 871 EL defect samples were available for MLP training and evaluation.

Defect(s)	$\mathbf{R^2}$	**MAE**
Crack, Contact, Interconnect, Corrosion	0.7865	0.6561
Crack Only	0.5269	0.8877
Contact Only	0.2015	1.6503
Interconnect Only	0.2406	1.5957
Corrosion Only	0.1042	1.6765

Table 1: MLP regression results for predicting current and voltage from EL defect data.

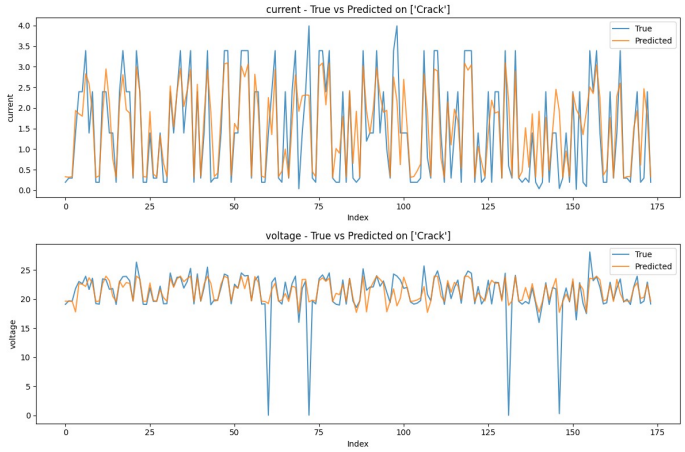

Fig. 5: Prediction of current and voltage using Crack defect

Crack defects yielded the highest predictive value among the individual defect types. However, the distribution of defects is uneven, with significantly more samples for cracks than for the other defects. As a result, these findings should be considered preliminary until more representative data is collected for contact, interconnect, and corrosion defects.

4.3 MLP (UVF Classification Data)

After preprocessing and filtering, only 78 valid UVF samples remained for training and evaluation. This limited dataset significantly constrained model performance.

- R^2 score: -0.0842
- MAE: 0.5811

These are the results using all 7 UVF defects to predict current and voltage. We suspect that the poor performance is caused by the lack of samples and believe that we can not meaningfully evaluate the viability of using UVF classification data until more samples are gathered.

4.4 LSTM

Signal Type	**R^2 Current**	**R^2 Voltage**	**MAE Current**	**MAE Voltage**
Raw measured signals	0.0888	0.5082	0.7657	3.3983
Wavelet transformed	0.3935	0.7717	0.2107	2.0932

Table 2: Performance metrics for LSTM predictions on raw vs. wavelet transformed voltage and current signals.

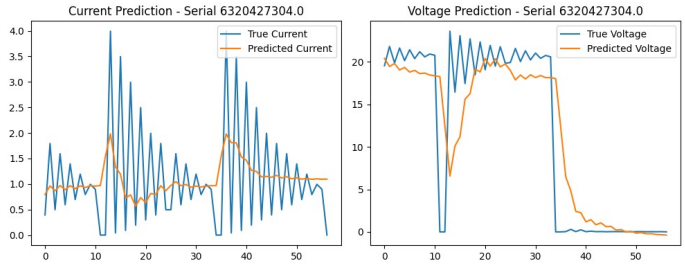

Fig. 6: Prediction for untransformed voltage and current signal

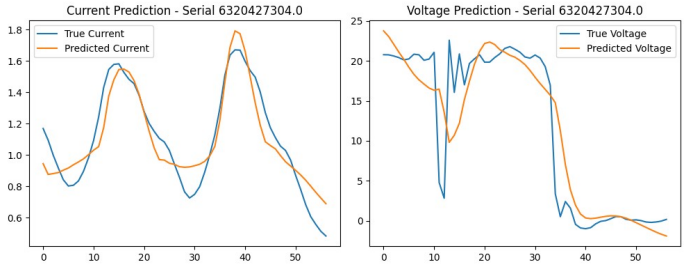

Fig. 7: Prediction for wavelet transformed voltage and current signal

The LSTM model demonstrated a notable improvement in performance when applied to wavelet-transformed signals compared to raw signals. As shown in Table 2, wavelet preprocessing led to significant increases in R^2 scores and reductions in MAE for both current and voltage predictions. This indicates that wavelet transforms effectively smooth the oscillatory behavior and reduce noise in the time series data, enabling the LSTM to learn more coherent patterns. However, it is important to note that these results were obtained under the simplifying assumption of uniformly spaced time intervals, which does not fully reflect the irregular and sparse nature of the original dataset. These findings suggest that wavelet-based pre-processing and LSTM architectures hold strong potential for modeling PV degradation over time, particularly in scenarios where measurements are consistently sampled. More robust performance could likely be achieved in future work with regularly spaced, high-frequency time-series data.

5 Conclusion

In this study, we developed a multi-modal deep learning pipeline to investigate how image-based features from electroluminescence (EL) and ultraviolet fluorescence (UVF) correlate with photovoltaic (PV) module performance. By aligning EL, UVF, and current-voltage (IV) data into a unified dataset, we explored several core research questions: which imaging modality and defect types best predict performance loss, and whether temporal patterns in IV signals can be modeled effectively over time.

Our results show that EL crack defects are the most predictive, yielding an R^2 of 0.53 in the crack-only MLP model, while the full-defect model achieved an R^2 of 0.79. UVF classification was less informative due to limited sample size. Time-series modeling using LSTM showed that wavelet-transformed IV signals significantly improved prediction accuracy compared to raw signals, raising R^2 from 0.09 to 0.39 for current and from 0.51 to 0.77 for voltage.

This work provides both a technical foundation and a reproducible workflow for future PV defect analysis. Some limitations remain, such as the imbalance of defect types and the irregularity of the time-series data. Future research should focus on expanding the dataset, improving UVF quality and quantity, and exploring pixel-level relationships with electrical features. Our foundational package is publicly available to support these next steps and accelerate progress in this area.

6 Acknowledgements

This research was conducted as part of the Data-Enabled Research Training and Development Sprints (DARTS) 2025 program, organized by the Data-Enabled Photovoltaics (UCF-DPV) Research Group at the University of Central Florida (UCF). We gratefully acknowledge the support of the Florida Solar Energy Center (FSEC), the Resilient, Intelligent and Sustainable Energy Systems (RISES) Research Center, and our collaborators at Case Western Reserve University.

References

[1] Colvin, D.J., Gabor, A.M., Oltjen, W.C., Knodle, P.J., Yao, A.D., Thompson, B.A., Khan, N., Lotfian, S., Raby, J., Jojo, A., Yu, X., Liggett, M., Seigneur, H.P., French, R.H., Bruckman, L.S., Li, M., Davis, K.O.: Ultraviolet fluorescence imaging for photovoltaic module metrology: Best practices and survey of features observed in fielded modules. IEEE Journal of Photovoltaics **15**(3), 465–477 (2025). https://doi.org/10.1109/JPHOTOV.2025.3545825

[2] Morlier, A., Siebert, M., Kunze, I., Mathiak, G., Köntges, M.: Detecting photovoltaic module failures in the field during daytime with ultraviolet fluorescence module inspection. IEEE Journal of Photovoltaics **7**(6), 1710–1716 (2017). https://doi.org/10.1109/JPHOTOV.2017.2756452

[3] Tsai, D.-M., Wu, S.-C., Li, W.-C.: Defect detection of solar cells in electroluminescence images using fourier image reconstruction. Solar Energy Materials and Solar Cells **99**, 250–262 (2012). https://doi.org/10.1016/j.solmat.2011.12.007. 9th International Meeting on Electrochromism

[4] Fioresi, J., Colvin, D.J., Frota, R., Gupta, R., Li, M., Seigneur, H.P., Vyas, S., Oliveira, S., Shah, M., Davis, K.O.: Automated defect detection and localization in photovoltaic cells using semantic segmentation of electroluminescence images. IEEE Journal of Photovoltaics **12**(1), 53–61 (2022). https://doi.org/10.1109/JPHOTOV.2021.3131059

[5] Chen, H., Zhao, H., Han, D., Liu, W., Chen, P., Liu, K.: Structure-aware-based crack defect detection for multicrystalline solar cells. Measurement **151**, 107170 (2020). https://doi.org/10.1016/j.measurement.2019.107170

[6] Tseng, D.-C., Liu, Y.-S., Chou, C.-M.: Automatic finger interruption detection in electroluminescence images of multicrystalline solar cells. Mathematical Problems in Engineering **2015**(1), 879675 (2015) https://onlinelibrary.wiley.com/doi/pdf/10.1155/2015/879675. https://doi.org/10.1155/2015/879675

[7] Lotfian, S., Ballen, A., Colvin, D.J., Khan, N., Thompson, B., Davis, K.O., Li, M.: Automatic classification of defects in solar photovoltaic panels using uv-fluorescence: A deep learning approach. In: 2024 IEEE 52nd Photovoltaic Specialist Conference (PVSC), pp. 1638–1641 (2024). https://doi.org/10.1109/PVSC57443.2024.10749318

Appendix A Appendix

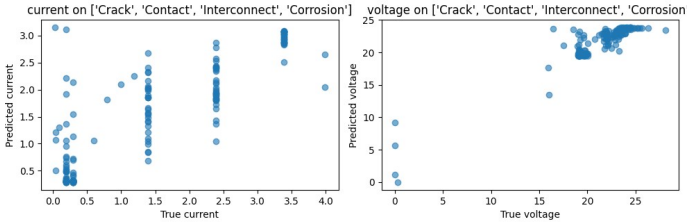

Fig. A1: MLP Prediction Graph 1 for All Defects

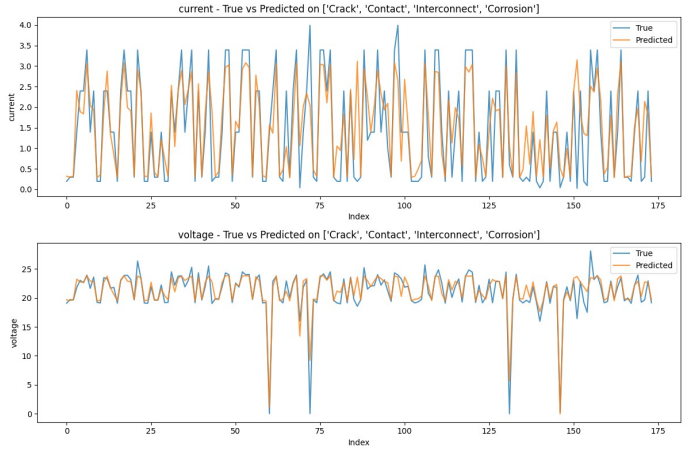

Fig. A2: MLP Prediction Graph 2 for All Defects

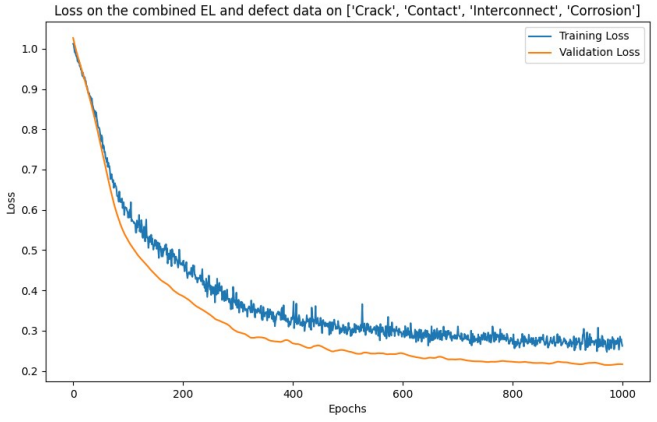

Fig. A3: MLP Training Loss Curve for All Defects

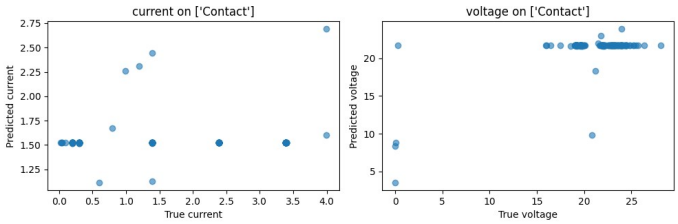

Fig. A4: MLP Prediction Graph 1 for Contact Defect

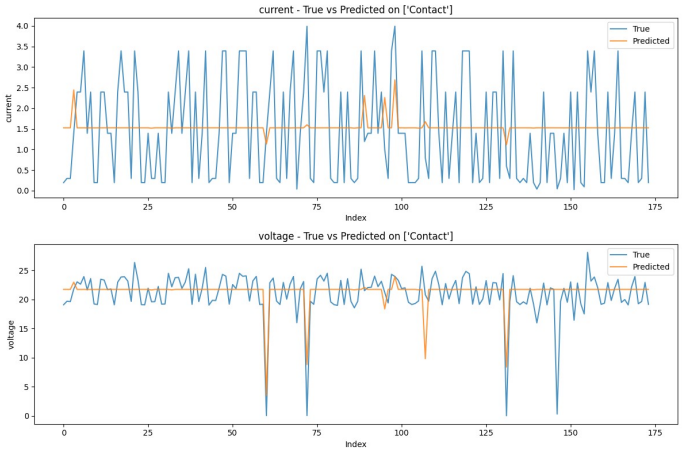

Fig. A5: MLP Prediction Graph 2 for Contact Defect

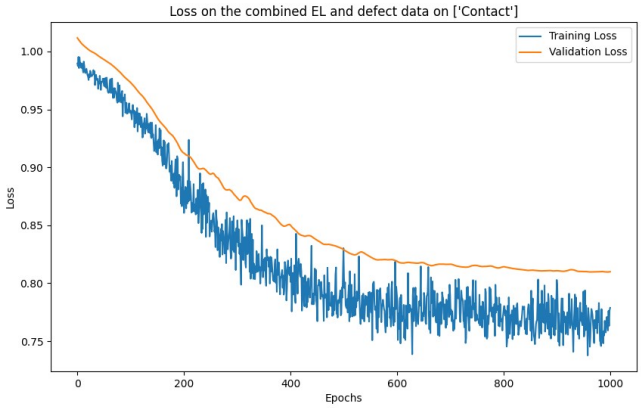

Fig. A6: MLP Training Loss Curve for Contact Defect

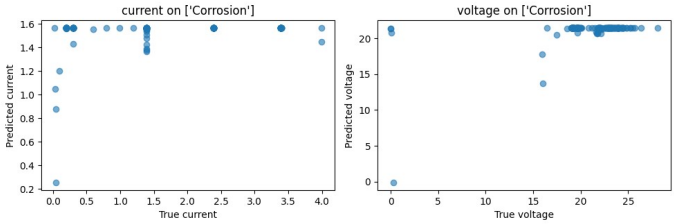

Fig. A7: MLP Prediction Graph 1 for Corrosion Defect

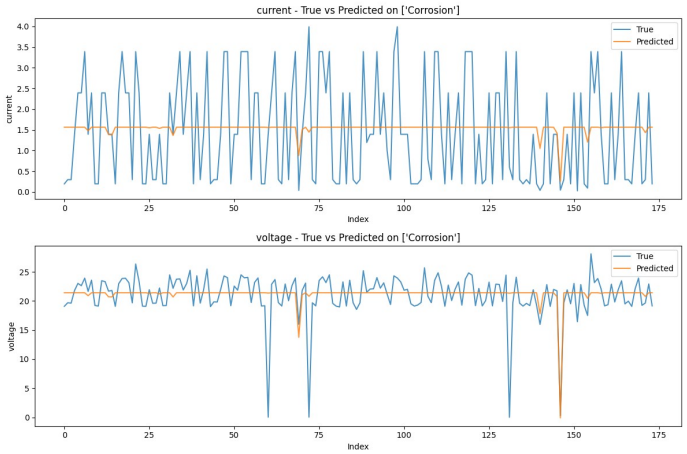

Fig. A8: MLP Prediction Graph 2 for Corrosion Defect

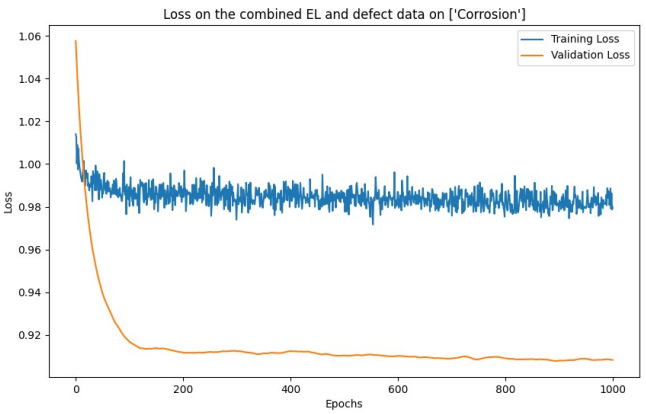

Fig. A9: MLP Training Loss Curve for Corrosion Defect

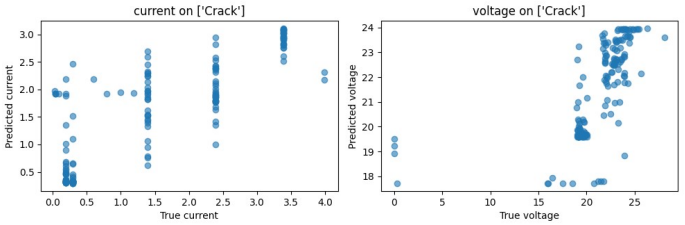

Fig. A10: MLP Prediction Graph 1 for Crack Defect

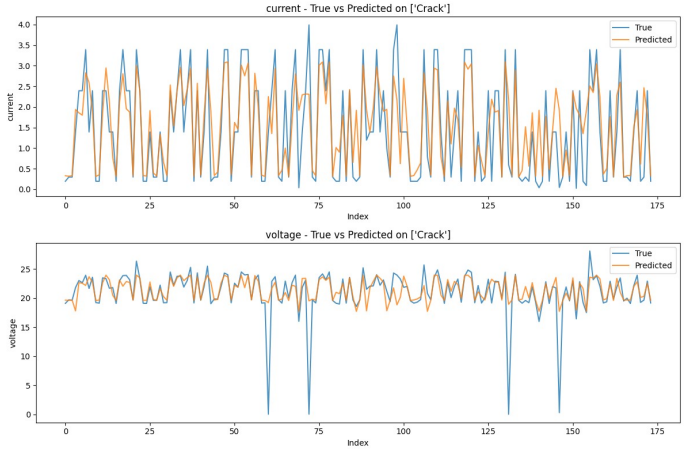

Fig. A11: MLP Prediction Graph 2 for Crack Defect

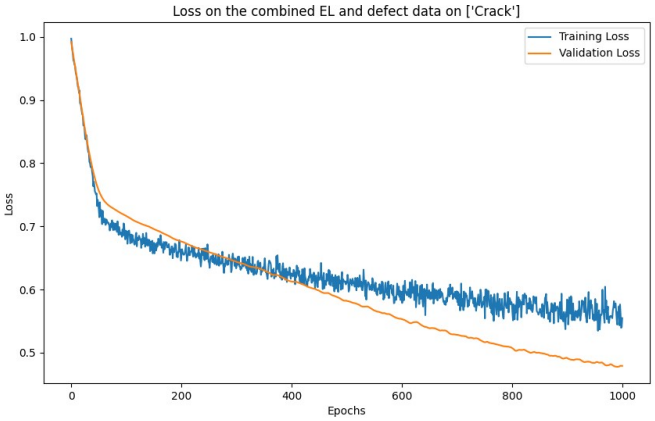

Fig. A12: MLP Training Loss Curve for Crack Defect

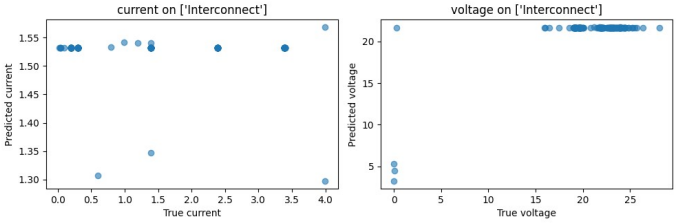

Fig. A13: MLP Prediction Graph 1 for Interconnect Defect

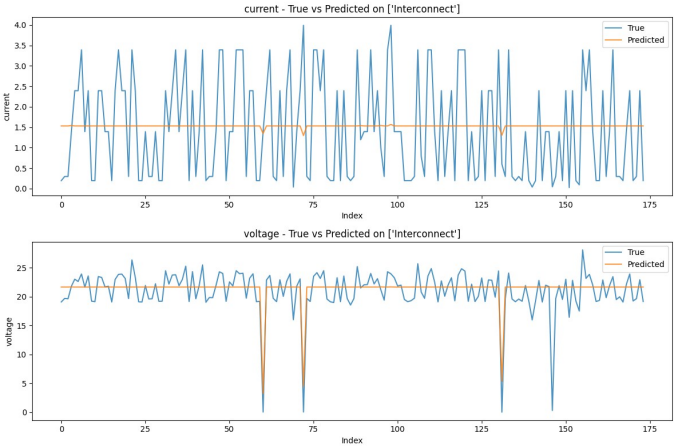

Fig. A14: MLP Prediction Graph 2 for Interconnect Defect

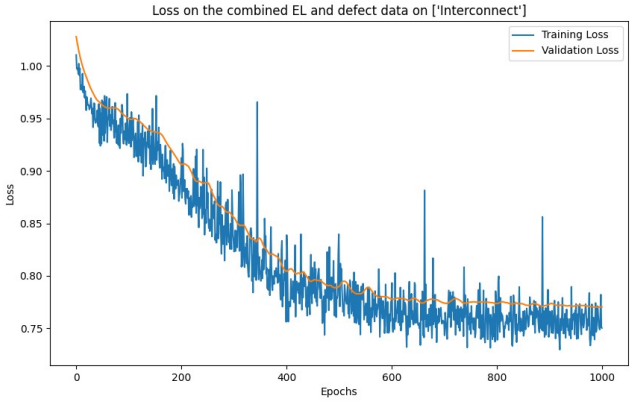

Fig. A15: MLP Training Loss Curve for Interconnect Defect

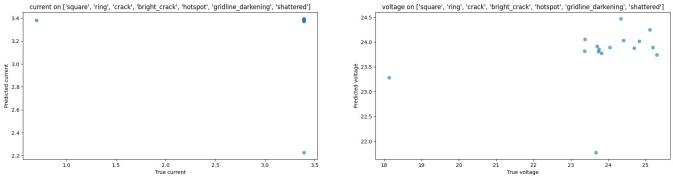

Fig. A16: MLP Prediction Graph 1 for UVF Combined Defect

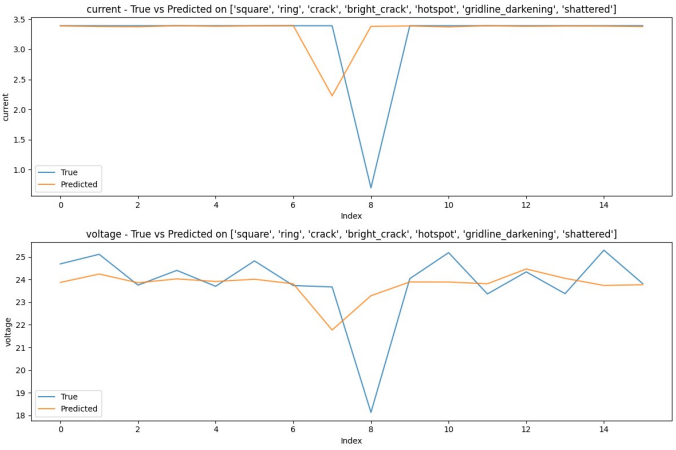

Fig. A17: MLP Prediction Graph 2 for UVF Combined Defect

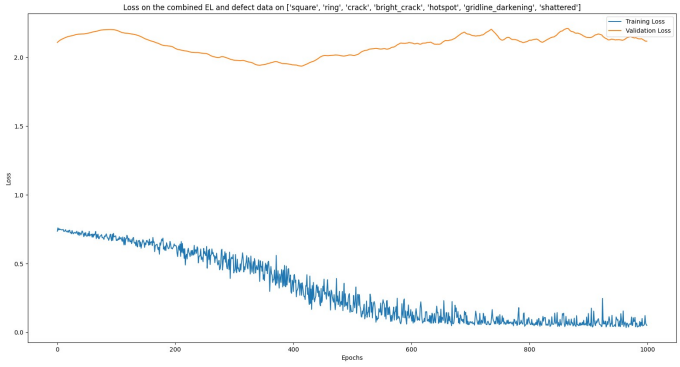

Fig. A18: MLP Training Loss Curve for UVF Combined Defect

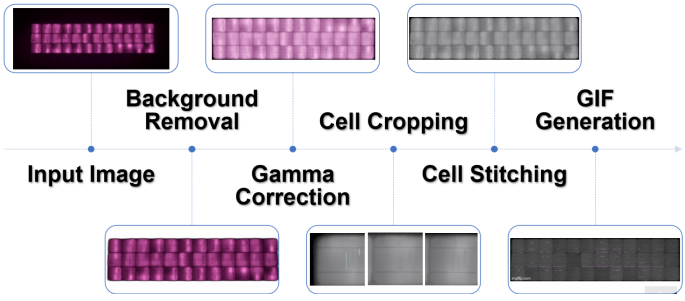

Fig. A19: The transformation from image to processed GIF